Optimization of Magnetic Susceptibility Weighted Imaging for Female Pelvic Scans

Wenjie Liu , Bin Yu , Furong Lv , Kaiwen Liang , Zhibo Xiao *

Posted Date: 7 June 2024

doi: 10.20944/preprints202406.0479.v1

Keywords: magnetic resonance imaging; magnetic susceptibility weighted imaging; flip angle; pelvic disease.

 doi:10.20944/preprints202406.0479.v1

Article

Optimization of Magnetic Susceptibility Weighted Imaging for Female Pelvic Scans

Wenjie Liu [1,†], Bin Yu [1,†], Furong Lv [1], Kaiwen Liang [2] and Zhibo Xiao[1,*]

[1] The Department of Radiology, The First Affiliated Hospital of Chongqing Medical University, Chongqing, China;
[2] The Department of Health Management , The First Affiliated Hospital of Chongqing Medical University, Chongqing, China.
* Correspondence: 202530@cqmu.edu.cn; Tel.+8617830038869
† These authors contributed equally to this work.

Abstract: *Background and Objectives*: The existing recommendations for female pelvic magnetic susceptibility weighted imaging MRI (FP-SWI) have not been optimized to capture the disease characteristics of the female pelvis. Therefore, it is imperative to explore acquisition parameters before conducting larger-scale studies. To establish optimized flip angle (FA) for acquiring FP-SWI to improve the image quality of female pelvic lesion sites. *Materials and Methods*: To evaluate signal quality and lesion conspicuity, regions of interest (ROIs) were manually drawn within the lesion on SWI sequences. Signal intensity was measured within the ROIs. Additionally, signal-to-noise ratio (SNR) and contrast-to-noise ratio (CNR) were calculated for SWI sequences acquired at three FA: 10°, 15°, and 20°. Finally, a qualitative assessment of anatomical detail visualization, geometric distortion extent, artifacts, and lesion clarity was performed using a four-point scale. The Wilcoxon rank sum test was employed to compare the qualitative evaluation parameters. The intra-class correlation coefficient (ICC) was calculated to determine the consistency of subjective ratings between two observers. *Results*: FA=10° showed significantly higher SNR than FA=15° and 20° in most anatomical regions ($P<0.05$), while the CNR was significantly higher than FA=15° and 20° ($P<0.05$). Compared with FA=15° and 20°, the image quality of FA=10° was significantly higher, with less distortion and ghosting, and better image contrast ($P<0.05$). Lesions with FA=10° exhibited higher clarity compared to FA=15° and 20° ($P<0.05$). *Conclusions*: The image quality of FP-SWI images at FA=10° exceeds that at FA=15° and 20°. We recommend that when conducting SWI examination of the female pelvic cavity, the FA value should be set at 10° to stabilize the SWI sequence and improve image quality.

Keywords: magnetic resonance imaging; magnetic susceptibility weighted imaging; flip angle; pelvic disease

1. Introduction

According to a survey conducted by the World Health Organization (WHO), the incidence of reproductive system diseases in Chinese women is as high as 87.8%. The main clinical symptoms include pain, abdominal distention, irregular menstrual cycles, and infertility[1]. These symptoms cause poor prognosis of patients and affect their physical and mental health, as well as imposing high economic burden.

MRI offers superior soft tissue contrast and is increasingly employed for pelvic examinations, particularly for disease localization and definitive diagnosis following initial US screening[2][3]. Currently, common methods for pelvic MRI examination include T1-weighted imaging (T1WI), T2-weighted imaging (T2WI), dynamic contrast-enhanced (DCE), perfusion-weighted imaging (PWI), diffusion-weighted imaging (DWI), and diffusion tensor imaging (DTI), which facilitate the diagnosis of pelvic hemorrhage diseases and tumor diseases such as endometriosis, uterine fibroids, ovarian tumor staging[4][5]. Clinical data indicate that bleeding in different periods cannot show the whole bleeding cycle on T1WI[6]. DWI sequences indicate subacute bleeding, however, the high signal of DWI is not specific to bleeding, as malignant tumors may also exhibit high signal, and low Apparent Diffusion Coefficient (ADC) reflects high expression of cancer tissue. This reveals that routine

 doi:10.20944/preprints202406.0479.v1

sequences cannot effectively differentiate issues such as hemorrhage staging, calcification, and iron deposition[7][8]. Therefore, SWI can be used for hemorrhage, calcification, iron deposition related diseases, and other areas.

SWI, as a functional MRI technique.It is widely used in brain and nervous system examination and fetal spine imaging[9][10][11]. Various fields use it to detect liver cirrhosis nodules, body tumor bleeding. Thus, it has become an effective imaging tool for detecting micro-bleeding, calcification and iron deposition, and is of great clinical significance [12][13]. However, the application of SWI for pelvis examination is limited, and recent studies have found that SWI can improve the detection of bleeding lesions such as endometriosis, adenomyosis, and uterine leiomyoma[14][15][16][17]. A study by However, this method is susceptible to magnetic artifacts and phase wrap artifacts[18][19]. The presence of intestinal gas artifacts caused by pelvic peristalsis and involuntary patient motion artifacts further lead to poor image quality, increasing the rate of clinical misinterpretation.

Previous studies have indicated that various MRI sequence parameters directly influences image quality, and the image quality of SWI is affected by parameters such as repetition time (TR), echo time (TE), and FA[20][21]. To reduce the scanning time and obtain a good T2* contrast, the generally accepted approach is to set the TR as short as possible. To achieve better phase contrast and accumulate a certain phase difference, TE is often chosen to be close to half of the T2* value of the tissue. At this point, the contrast of the SWI image is no longer determined by TR and TE, but by FA[22]. Ashmita De et al.[23] found that increased FA may decrease background tissue SNR, inducing artifacts in Quantitative susceptibility mapping (QSM). FA=18° is selected to achieve appropriate contrast of TOF-MRA arteries and appropriate tissue signal-to-noise ratio of SWI/QSM. Lower FA can improve interstitial SNR without decreasing interstitial contrast. Gesine Knobloch et al.[24], found that the IVC filter description and vein image quality were best at a low FA of 10°, while a higher FA increased image noise in Ultrashort Echo Time Magnetic Resonance Angiography (UTE-MRA) for inferior vena cava imaging. Vanessa Franziska Schmidt et al.[25] found that higher FA in real-time T1WI Gradient Recalled Echo (T1WIGRE) sequences for MR-guided liver interventions resulted in more severe artifacts, which is consistent with findings from another research[26]. Other studies have shown[27][28][29] that an appropriate FA value can improve the contrast of specific contrast agents, liver and biliary tract images, and enhance the detection of focal liver lesions. Currently, there are no reports on the application of SWI in parameter optimization for female pelvic scanning. Therefore, we aimed to solve the problems of poor image quality and serious artifacts by optimizing FA to improve image quality.

2. Materials and Methods

Study Population

The study was approved by the Local Ethics Committee (application no: 2023-359), and informed consent was obtained from each participant. All patients diagnosed with female pelvic disease who underwent total abdominal or lower abdominal and pelvic MRI (including SWI) between September 2023 and January 2024 were enrolled in this study (Figure 1). The eligible patients were those who have previously been treated (have not had a hysterectomy) and those with untreated disease. Those who did not undergo scanning were excluded. The patients received routine MRI sequences and SWI sequences (three FA selections were collected at 10°, 15°, and 20°). While a smaller flip angle (FA=5°) did not improve SNR and CNR compared to a larger angle (FA=10°) and impaired T1 contrast and saturation recovery.In SWI, the FA is a critical parameter that influences image contrast. Choosing an excessively low FA can lead to SWI images dominated by T2 signal, while excessively high FA can lead to T1-weighted bias*. In female pelvic MRI, typical FA values for SWI range from 15° to 20° to achieve optimal contrast. Here, we opted for a graded approach, systematically acquiring SWI images at decreasing FA values with a step size of 5° using a 3.0T scanner (GE Signa Pioneer Healthcare, Waukesha, WI, USA) (Table 1).

 doi:10.20944/preprints202406.0479.v1

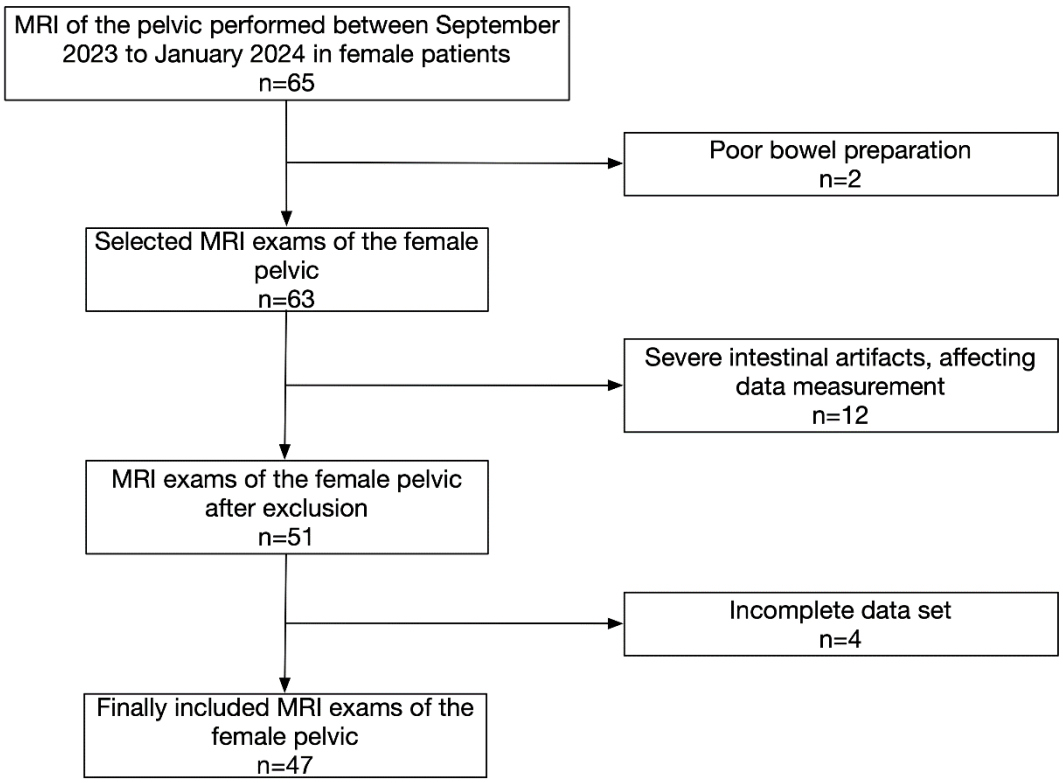

Figure 1. Flow diagram of the study design.

Table 1. MRI acquisition parameters.

Scanning parameters	SWI	T2	T2WI	T1WI	DWI	LAVA
		Abdo			pelvis	
Patients		17			30	
B0 field strength(T)			3.0			
Scanner model			SIGNA Pioneer			
Sequence	3D SPGR	FRFSE	FRFSE	SPGR	EPI	3D GRE
Orientation	Axial	Sagittal	Axial	Axial	Axial	Axial
Echo time(ms)	Out of phase	85	98	In Phase	Minimum	1.9
Repetition time(ms)	Minimum	3761	2509	150	5490	4.1
Slice thickness(mm)	3	4	4.0	5.0	4.0	3.6
Slice gap(mm)	0	1.0	1.0	1.5	1.0	0
Field of view(mm)	300	240	240	380	380	380
Bandwidth	31.25	35.71	41.67	83.33	250	83.33
NEX		1	2	1	4	
Acquisition matrix	360×300	320×256	360×256	320×224	128×128	320×288
Breathing instructions	Free	Free	Free	Free	Free	Free
Flip angel	10、15、20	140	140	70		12

All scanners made by GE Healthcare. SPGR,Spoiled Gradient Echo; FRFSE, Fast Recovery Fast Spin Echo; EPI,Echo Planar Imaging ; 3D GRE, Gradient Echo.

 doi:10.20944/preprints202406.0479.v1

Image and Data Analysis

For each patient, the smallest lesion diameter of 0.5 ~ 1.5 cm^2 was selected as the ROI on the intermediate layer image slices containing lesions to avoid partial volume effects and examined by a radiologist with more than 1 year of FP-SWI experience (Figure 2).The ROI was plotted using the GE post-processing workstation AW4.7 and the morphological sequence was used as a reference. A minimum lesion diameter of 0.5 to 1.5cm^2 was selected as the ROI to avoid partial volume effects.

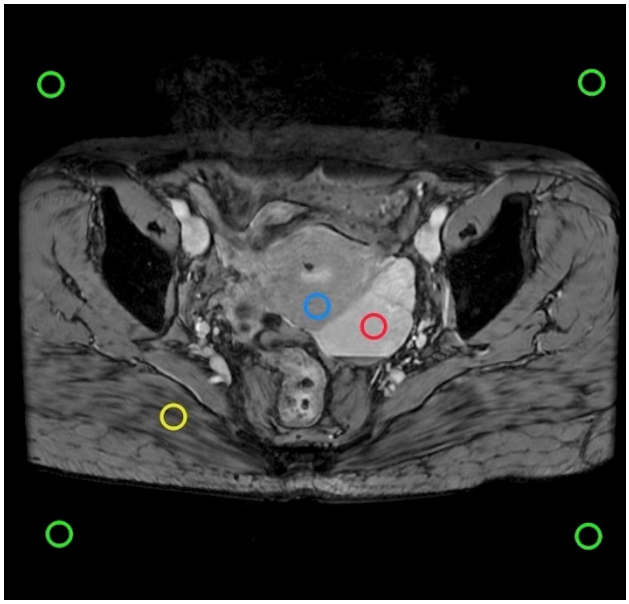

Figure 2. In the SWI intermediate layer, ROI (green) examples are plotted to estimate noise. Lesions are depicted in red, the uterus in blue, and the gluteus maximus in yellow. The pixel count within the ROI remains constant across different matrix sizes.

To determine the optimal FA, absolute SNR_{abs} and CNR_{abs} calculations were performed from the ROI measurements of the three measured FAs. SNR_{abs} were calculated for each subject using the formula:

$$SNR_{abs} = SI_{tissue}/STD_{air} \times 0.7049 \quad (1)$$

SI_{tissue} is the average SI in the relevant tissue and STD_{air} is the standard deviation of the air signal. For amplitude images obtained using multi-channel coils, the correction coefficient (0.7049) was selected to explain the difference in noise variance behavior in the background [30]. The signal intensity (SI) was measured by placing ROI on the lesion, gluteus maximus and myometrius respectively, ranging from 0.5 to 1.5cm^2, and the measurement was averaged three times. CNR_{abs} calculations were used to compare lesions and contrast between the gluteus maximus and the uterus：

$$CNR_{abs} = SNR_{focus} - SNR_{tissue} \quad (2)$$

Image evaluation was performed by two blinded radiologists with expertise in gynecologic MRI. One radiologist possessed 18 years of experience, while the other had 8 years of experience. Neither radiologist had access to clinical or pathological patient information to minimize bias. A four-point Likert scale adapted from Hellms et al. [31] was used to assess image quality across four domains: anatomical detail visualization, geometric distortion, artifact presence, and lesion conspicuity. The specific scoring criteria were as follows: anatomical detail display (1=poor, 2=fair, 3=good, 4=excellent); degree of geometric distortion (1=severe, 2=moderate, 3=mild, 4=none); artifacts (1=severe, 2=moderate, 3=mild, 4=absent); clarity of lesions (1=poor, considered unidentified; 2=moderate, most contours unclear; 3=good, some contours unclear; 4=excellent, clear contours).

 doi:10.20944/preprints202406.0479.v1

Statistical Analysis

All statistical analyses were performed using SPSS (IBM SPSS Statistics for Macintosh，version 26.0). Measurements of image SNR and CNR were conducted at FA (10°, 15°, 20°), and analyzed by paired t-tests, Wilcoxon rank-sum tests, repeated measures ANOVA (with Bonferroni correction), or Friedman tests. The Wilcoxon rank sum test was employed to compare the qualitative evaluation parameters. The ICC was calculated to determine the consistency of subjective ratings between two observers (ICC>0.75 indicated good consistency, 0.50≤ICC≤0.75 indicated moderate consistency, ICC<0.50 indicated poor consistency). P<0.05 was considered statistically significant.

3. Results

1. Research population

Forty-seven female patients with pelvic diseases underwent MRI examination, with an average age of (45.81±13.07) years. Among them, 17 patients received a full abdominal scan, while 30 patients underwent lower abdominal and pelvic scans.

2. Clinical evaluation

The distribution of the lesions is shown in Table 2. A total of 55 lesions were analyzed in this study. The most common lesions were endometriosis, uterine fibroids, and ovarian cysts. Of these, 16/55 (29.10%) patients had different types of endometriosis (mainly adenomyosis and endometriosis cysts), 13/55 (23.64%) patients had uterine fibroids (mainly intermuscular and posterior wall fibroids), 8/55 (14.55%) patients had ovarian cysts (luteal cysts and mesosalpingal cysts), 8/55 (14.55%) patients were detected with cystadenomas (serous and mucous), 6/55 (10.90%) patients had cervical cysts of various types, 2/55 (3.63%) patients had teratoma, and 2/55 (3.63%) patients showed cervical cancer.

Table 2. Clinical characteristics of the study population.

Characteristic		N（type）	Total
Age（years）		45.81±13.07	
N（patient）		47	
N（lesion）		55	
Endometriosis	Ectodermatosis	9	16
	Adenomyosis	6	
	Rectal endometriosis	1	
Hysteromyoma	Intramural	5	13
	Anterior	2	
	Posterior	5	
	Fundal	1	
Ovarian cysts	Luteum cyst	3	8
	Mesangial cyst	3	
	Other	2	
Cystadenoma	Serous	5	8
	Mucinous	3	
Cervical cysts		6	6
Teratoma		2	2
Cervical cancer		2	2
Total（lesion）		55	55

3. Image analysis

In this study, the overall scan time was 13'04", and SWI scans were completed within a reasonable time frame after performing routine MR sequences.Two independent observers evaluated the image quality of SWI sequences acquired at three flip angles (FA): 10°, 15°, and 20°. Their assessment focused on anatomical detail visualization, geometric distortion extent, artifact presence, and lesion conspicuity. High inter-rater reliability was achieved, as demonstrated by the strong consistency between observers' scores (Table 3). Statistical analysis revealed significant differences

 doi:10.20944/preprints202406.0479.v1

(P< 0.05) in all these qualitative and quantitative metrics across the three FA values. Pelvic anatomical details evaluated by the Likert scale revealed that the mean ±SD score was 3.7±0.6 at FA=10°, 3.2±0.6 at FA=15°, and 2.7±0.8 at FA=20°. Regarding the degree of deformation, significant differences were observed between the measurement series (P < 0.0001), with the Likert scale averaging ±SD scores of 3.6±0.6 at FA=10°, 3.4±0.7 at FA=15°, and 3.1±0.8 at FA=20°.There were significant differences in the degree of artifact among the FAs (P < 0.0001), with more severe artifacts detected among the higher FAs, with an average ±SD score of 3.5±0.8 at FA=10°, 3.2±0.8 at FA=15°, and 2.8±0.9 at FA=20°. In terms of lesion clarity, significant differences were observed between the selected FAs (P < 0.0001), with a mean ±SD score of 3.6±0.6 at FA=10°, 3.2±0.6 at FA=15°, and 2.8±0.7 at FA=20°. Consistency of the subjective scores of the other groups was good (ICC > 0.75), except for the degree of degeneration of FA=15° and 20° (ICC=0.75).

Table 3. Qualitative evaluation of SWI sequences with different flip angles (10°, 15°, 20°).

Parameter	Reader	FA			*p*
		10°	15°	20°	
Anatomical details	**Reader1**	**3.7±0.5ab**	**3.1±0.6 b**	**2.8±0.8**	**<0.0001**
	Reader2	**3.7±0.7 ab**	**3.3±0.7 b**	**2.6±0.8**	**<0.0001**
	ICC	**0.903**	**0.873**	**0.784**	
Geometric deformation	**Reader1**	**3.6±0.6 ab**	**3.4±0.7 b**	**3.0±0.9**	**<0.0001**
	Reader2	**3.5±0.6 ab**	**3.3±0.7 b**	**3.1±0.7**	**<0.0001**
	ICC	**0.919**	**0.759**	**0.756**	
Artifact	**Reader1**	**3.5±0.7 ab**	**3.1±0.7 b**	**2.7±0.9**	**<0.0001**
	Reader2	**3.5±0.8 ab**	**3.3±0.8 b**	**2.8±0.9**	**<0.0001**
	ICC	**0.907**	**0.862**	**0.827**	
Lesion resolution	**Reader1**	**3.6±0.6 ab**	**3.1±0.6 b**	**2.7±0.7**	**<0.0001**
	Reader2	**3.6±0.6 ab**	**3.3±0.5 b**	**2.8±0.7**	**<0.0001**
	ICC	**0.867**	**0.785**	**0.896**	

* represents statistical significance.a represents statistical difference compared with the FA=15°group, and b represents statistical difference compared with the FA=20°group (after Bonferroni correction for multiple comparisons). Values are given as mean ± standard error of the mean. A 4-point Likert-scale was applied for the visual assessment of image quality: 1=non-diagnostic, 2=poor, 3=satisfactory, 4=good. P-values were derived from Wilcoxon rank sum tests. ICC = intraclass correlation coefficient.

SNR and CNR of various anatomical positions and disease sites under different FA values are shown in Table 4. Similar results were obtained in the quantitative assessments of signal strength, and there were significant differences between SNR (lesion, gluteus maximus, uterus) and CNR (lesion) in the selected FAs (P<0.001, P<0.003). When FA=10°, SNR (lesion, gluteus maximus, uterus) was the highest compared with the other two groups. When FA=10°, CNR (lesion) was the highest compared with the other two groups. Regarding lesion SNR measurement, there was a significant difference between the selected FAs (P<0.001), with the mean SNR being 129.31±30.33 at FA=10°, 107.06±31.64 at FA=15°, and 92.77±33.43 at FA=20°. For SNR measurements of gluteus maximus, there were significant differences between the measurement sequences (P<0.001), with the mean SNR of 62.58±15.60 at FA=10°, 54.19±14.74 at FA=15°, and 46.31±12.33 at FA=20°.Concerning uterine SNR measurements, significant differences were observed among FAs (P<0.001), with a mean SNR of 105.37±22.43 at FA=10°, 92.38±22.89 at FA=15°, and 83.04±24.88 at FA=20°. Significant differences were recorded in CNR among the selected FAs (P<0.003). The mean CNR was 67.12±25.01 at FA=10°, 53.66±27.20 at FA=15°, and 47.05±30.27 at FA=20°.

 doi:10.20944/preprints202406.0479.v1

Table 4. Comparison of image data values for different flipping angles in SWI sequences.

Variables		N	FA			F	*p*
			10°	15°	20°		
SNR	lesion	55	129.31±30.33ab	107.06±31.64	92.77±33.43	14.729	<0.0001
	ectogluteus	55	62.58±15.60 ab	54.19±14.74[b]	46.31±12.33	17.834	<0.0001
	uterus	55	105.37±22.43 ab	92.38±22.89	83.04±24.88	10.089	<0.0001
CNR	lesion	55	67.12±25.01 ab	53.66±27.20	47.05±30.27	6.056	0.003*
	uterus	55	43.71±21.17	37.04±15.54	36.07±17.54	2.293	0.105

* represents statistical significance. a represents statistical difference compared with the FA=15°group, and b represents statistical difference compared with the FA=20°group (after Bonferroni correction for multiple comparisons).

4. Discussion

This study investigated the potential for optimizing FA in SWI protocols for female pelvic examinations. Our findings demonstrate the feasibility of FA optimization to enhance image quality and potentially improve diagnostic accuracy in the context of uterine diseases. Moreover, we found that a low flip angle (FA=10°) provided the best image quality for the SWI sequence.

Regarding FA, lower FA revealed more anatomical detail and lesion clarity, less deformation and artifacts, and 10° had the best effect compared to 15° and 20°. The score for anatomical details and lesion clarity for FA=10° were significantly higher compared to those of FA=15° and 20°, indicating that the anatomical details and lesion clarity were highest at 10° (Figure 3). For the degree of deformation and ghosting, the subjective rating for FA=10° was higher than that of FA=15° and 20°, suggesting that the degree of deformation and ghosting was smallest at 10° (Figure 4), while the degree of deformation and ghosting was the most severe at 20°. Qualitative assessment revealed superior image quality at a FA of 10° compared to 15° and 20°. Images acquired at FA=10° demonstrated improved visualization of small hemorrhagic lesions, clearer delineation of peritumoral infiltration in tumors, and enhanced depiction of pelvic anatomical structures. Moreover, image quality was superior in the FA=10° scans compared to FA=15° and 20° scans, likely attributable to the substantial difference in signal intensity between focal lesions and surrounding tissues. This heightened level of detail is crucial for accurate diagnosis and selection of optimal treatment strategies.

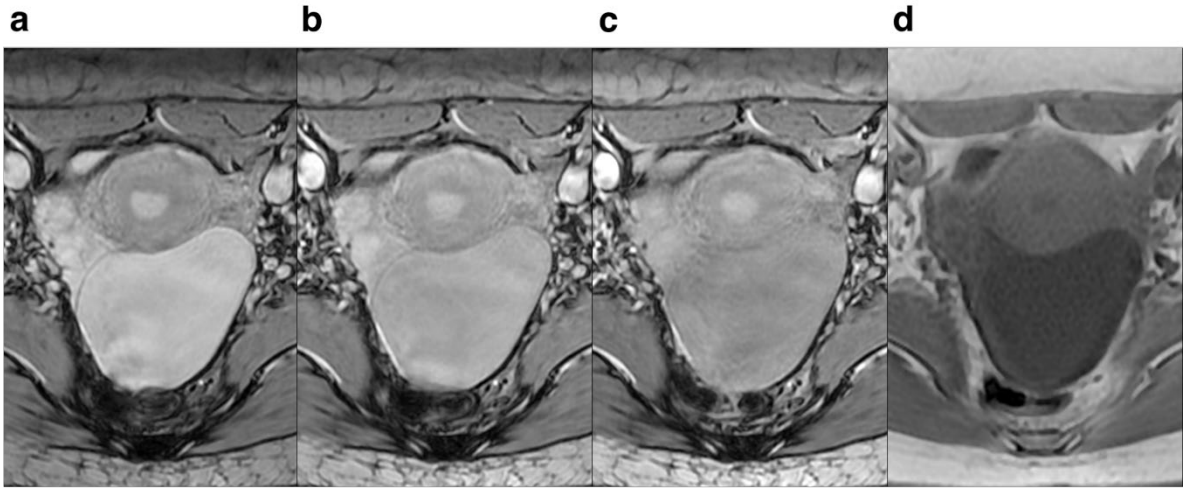

Figure 3. Female, 30 years old. Pelvic cavity under each FA is shown. SWI sequences FA were 10° (a), 15° (b), 20° (c),and T1WI(d) respectively.It can be seen that when FA=10°, the pelvic structure is more clearly displayed and the lesion is more clearly outlined than the other FA.

 doi:10.20944/preprints202406.0479.v1

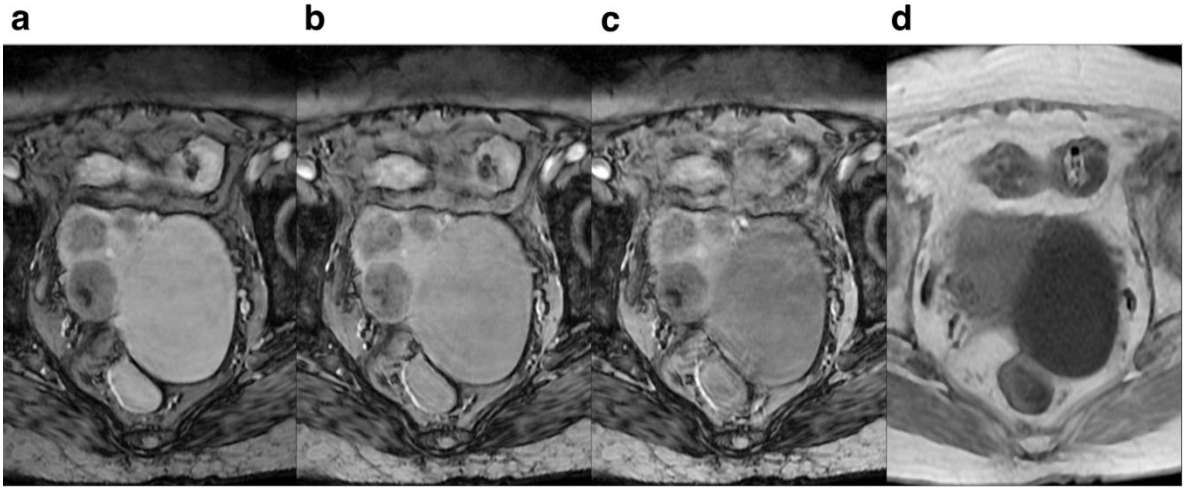

Figure 4. Female, 83 years old. Pelvic cavity under each FA is shown. SWI sequences FA were 10° (a), 15° (b) ,20° (c) and T1WI (d),respectively. It can be seen that when FA=10°, the pelvic structure has less deformation and less artifacts than the other FA.

Our results indicated that SNR and CNR in each part of pelvic cavity increased in a step-wise manner with the decrease of FA from 20° to 10°(Figure 5), but the increase was not significant when FA=20°. Notably, FA=10° was significantly different between the two groups, but not between FA=15° and 20°. The decrease in signal strength observed at higher FAs (likely exceeding the Ernst angle) can be attributed to limitations inherent in the spoiled gradient echo (SPGR) sequence used for signal acquisition. According to the principles governing SPGR sequences with fixed TR and T1 values, increasing FA leads to a larger initial horizontal magnetization component, which typically translates to stronger signal intensity. However, excessively high FAs can compromise longitudinal relaxation within the fixed TR. This insufficient recovery time prevents the full return of the longitudinal magnetization vector along the z-axis, ultimately leading to a net decrease in detectable signal. Following re-excitation, the magnetization vector was partially saturated. As the angle increases, the signal strength gradually decreases. Therefore, for any tissue with a known T1 value and a fixed TR value, it has an optimal FA that maximizes the signal intensity at that angle, known as the Ernst angle [32,33]. When the FA is higher than the Ernst angle, the magnetization vector is partially saturated, in which decreases the signal intensity. In female pelvic imaging, the SNR and CNR of the pelvis increase in a step-like manner as the FA decreases, reaching a maximum value at FA=10°. This is because decreasing FA can increase the signal intensity of short T2 tissues and reduce the signal intensity of long T2 tissues [34], thereby increasing the contrast between different parts of the pelvis and improving the image quality.

 doi:10.20944/preprints202406.0479.v1

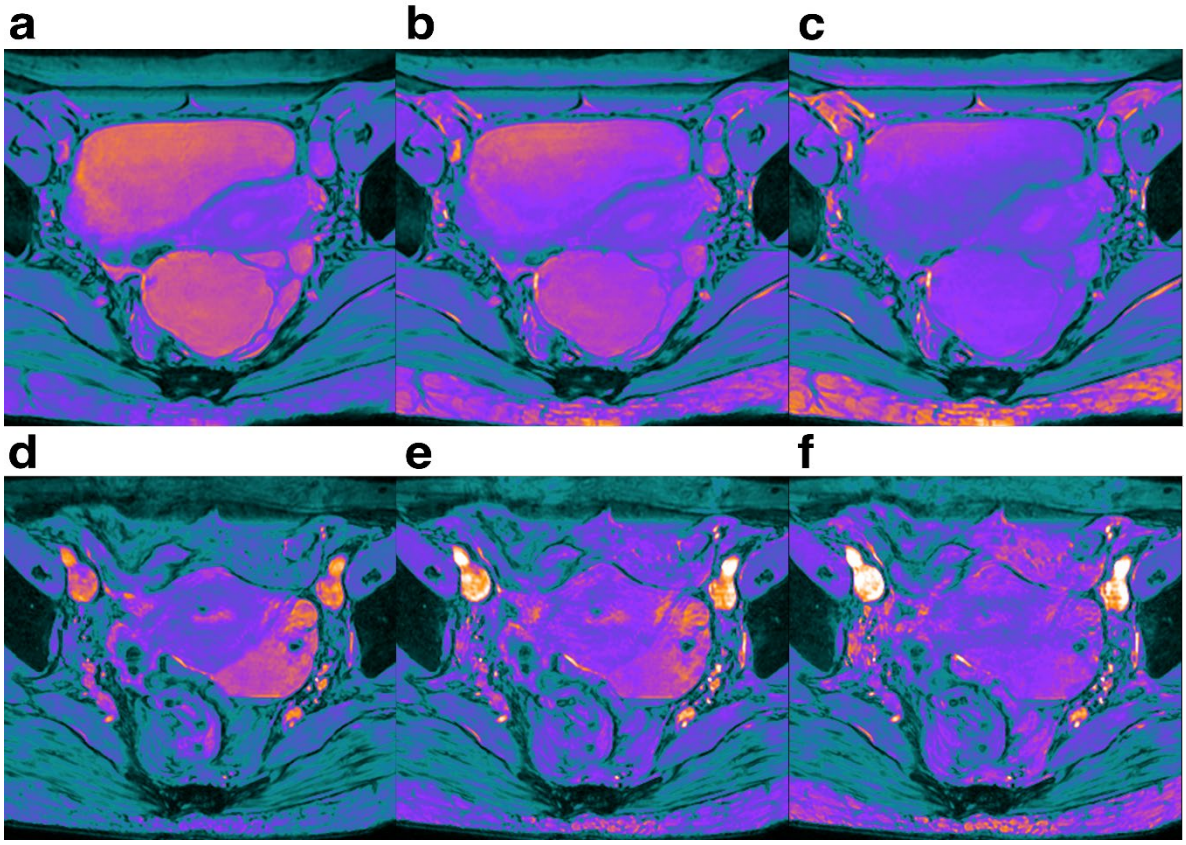

Figure 5. Female,Pelvic cavity under each FA is shown. The SWI sequences before injection were 10° (a,d), 15° (b,e) and 20° (c,f), respectively. It can be seen that when FA=10°, the SNR and CNR of pelvic structure are higher than those of the other two groups.

This prospective study of female patients with pelvic disease found that SNR and CNR were significantly different in terms of lesion and anatomical site under different FA values, and the overall mean SNR and CNR values were calculated. Our analysis suggests that a 10° FA represents a practical optimal value for SWI imaging in the female pelvis. Higher FAs (>10°) can lead to reduced signal intensity in pelvic pathologies, particularly those with low T2-weighting. This, in turn, can introduce noise bias into SNR and CNR measurements. At higher FA values, the decrease in signal and increase in the distortion may decrease the image signal strength and loss of image quality. The larger the FA value, the heavier the MTC magnetization transfer effect is, and the contrast of the image containing protein decreases[34].While a 10° FA may not be ideal for every pathology, it offers a valuable compromise by minimizing noise bias in these low-signal regions, ultimately enhancing diagnostic accuracy.

Considering that gadolinium contrast agent injection can affect the magnetization characteristics of tissues, and T2 and T1 relaxation[35], to maintain good visualization of female pelvic lesions, we performed the scans before injection of gadolinium contrast agent. Consequently, the relationship between different FA values and the imaging quality of female pelvic scans, which is more clinically relevant, is discussed in this study.

The key limitation of this study is that the prospective data used was highly heterogeneous due to variations in the scanner, field strength and parameters. While these differences may affect properties such as SI, SNR, and CNR, the differences between parameters are relatively small. In addition, we enrolled a relatively small sample size of 45 cases, and this may bias the results.

Moreover, with the advent of high intensity focused ultrasound (HIFU) therapy [36], the proportion of female pelvic patients receiving HIFU therapy has been on the raise. Therefore, the characteristics of women's pelvic lesions before and after treatment should be considered to ensure

 doi:10.20944/preprints202406.0479.v1

that the image quality obtained by the recommended FA values is appropriate for this group of patients at all stages of treatment.

5. Conclusions

When SWI is performed in women with pelvic disease, we recommend that the FA value should be selected to 10° to stabilize SWI sequence and improve image quality, and hence the diagnosis of female pelvic diseases.

Author Contributions: Conceptualization, Wenjie Liu, Furong Lv and Zhibo Xiao; Data curation, Wenjie Liu; Formal analysis, Wenjie Liu and Kaiwen Liang; Funding acquisition, Zhibo Xiao; Investigation, Wenjie Liu; Methodology, Wenjie Liu and Bin Yu; Project administration, Furong Lv and Zhibo Xiao; Resources, Bin Yu and Furong Lv; Supervision, Furong Lv and Zhibo Xiao; Validation, Wenjie Liu and Bin Yu; Visualization, Wenjie Liu; Writing – original draft, Wenjie Liu; Writing – review & editing, Wenjie Liu, Bin Yu and Zhibo Xiao.

Funding: Please add: "This research received no external funding" or "This research was funded by NAME OF FUNDER, grant number XXX" and "The APC was funded by XXX". Check carefully that the details given are accurate and use the standard spelling of funding agency names at https://search.crossref.org/funding. Any errors may affect your future funding.

Institutional Review Board Statement: The study was conducted in accordance with the Declaration of Helsinki, and approved by the Institutional Review Board (or Ethics Committee) of The First Affiliated Hospital of Chongqing Medical University (protocol code 2023-359 , October 16, 2023)." for studies involving humans.

Informed Consent Statement: Informed consent was obtained from all subjects involved in the study. Written informed consent has been obtained from the patient(s) to publish this paper.

Data Availability Statement: The datasets used and/or analysed during the current study available from the corresponding author on reasonable request.

Acknowledgments: This project was sponsored by Chongqing Medical University Program for Youth Innovation in Future Medical (w0107).

Conflicts of Interest: The authors declare no conflicts of interest.

References

1. Sudderuddin S, Helbren E, Telesca M, Williamson R, Rockall A. MRI appearances of benign uterine disease. Clin Radiol. 2014;69(11):1095-1104.
2. Bazot M, Thomassin I, Hourani R, Cortez A, Darai E. Diagnostic accuracy of transvaginal sonography for deep pelvic endometriosis. Ultrasound Obstet Gynecol. 2004;24(2):180-185.
3. Redpath TW. MRI developments in perspective. Br J Radiol. 1997;70 Spec No:S70-S80.
4. Bazot M, Bharwani N, Huchon C, et al. European society of urogenital radiology (ESUR) guidelines: MR imaging of pelvic endometriosis. Eur Radiol. 2017;27(7):2765-2775.
5. Guerra A, Daraï E, Osório F, et al. Imaging of postoperative endometriosis. Diagn Interv Imaging. 2019;100(10):607-618.
6. Bradley WG Jr. MR appearance of hemorrhage in the brain. Radiology. 1993;189(1):15-26.
7. Holland, B A et al. "MR imaging of calcified intracranial lesions." Radiology vol. 157,2 (1985): 353-6.
8. Hernando, Diego et al. "Quantification of liver iron with MRI: state of the art and remaining challenges." Journal of magnetic resonance imaging : JMRI vol. 40,5 (2014): 1003-21.
9. Haller S, Haacke EM, Thurnher MM, Barkhof F. Susceptibility-weighted Imaging: Technical Essentials and Clinical Neurologic Applications. Radiology. 2021;299(1):3-26.
10. Liu S, Buch S, Chen Y, et al. Susceptibility-weighted imaging: current status and future directions. NMR Biomed. 2017;30(4):10.1002/nbm.3552.
11. Franco PN, Annibali S, Viganò S, et al. T2*-Weighted Imaging Performance in the Detection of Deep Endometriosis among Readers with Different Experience: Comparison with Conventional MRI Sequences. Diagnostics (Basel). 2022;12(7):1545.
12. Haacke EM, Mittal S, Wu Z, Neelavalli J, Cheng YC. Susceptibility-weighted imaging: technical aspects and clinical applications, part 1. AJNR Am J Neuroradiol. 2009;30(1):19-30.
13. Mittal, S., Wu, Z., Neelavalli, J., & Haacke, E. M. (2009). Susceptibility-weighted imaging: technical aspects and clinical applications, part 2. AJNR. American journal of neuroradiology, 30(2), 232–252.
14. Takeuchi M, Matsuzaki K, Nishitani H.Susceptibility weighted MRI of endometrioma： preliminary results.AJR, 2008, 191:1366-1370.

 doi:10.20944/preprints202406.0479.v1

15. Takeuchi M, Matsuzaki K, Harada M.Susceptibility-weighted MRIof extra-ovarian endometriosis:preliminary results.Abdom Imaging, 2015, 40:2512-2516.
16. Pin L, Monseau-Thiburce AC, Ziade-Coularis C, et al. Exploratory study of the interest of MR susceptibility-weighted imaging for the pre-operative assessment of pelvic endometriosis extent. Eur J Radiol. 2019;118:245-250.
17. Guerriero S, Ajossa S, Pagliuca M, et al. Advances in Imaging for Assessing Pelvic Endometriosis. Diagnostics (Basel). 2022;12(12):2960.
18. Kim HS, Jahng GH, Ryu CW, Kim SY. Added value and diagnostic performance of intratumoral susceptibility signals in the differential diagnosis of solitary enhancing brain lesions: preliminary study. AJNR Am J Neuroradiol.2009;30(8):1574-1579.
19. Chen H, Wang G, Wang X, Gao Y, Liang J, Wang J. Diagnostic value of susceptibility-weighted imaging for endometrioma: preliminary results from a retrospective analysis. Acta Radiol. 2022;63(7):976-981.
20. Nandigam RN, Viswanathan A, Delgado P, et al. MR imaging detection of cerebral microbleeds: effect of susceptibility-weighted imaging, section thickness, and field strength. AJNR Am J Neuroradiol 2009;30(2):338–343.
21. Halefoglu AM, Yousem DM. Susceptibility weighted imaging: Clinical applications and future directions. World J Radiol. 2018;10(4):30-45.
22. Haller S, Haacke EM, Thurnher MM, Barkhof F. Susceptibility-weighted Imaging: Technical Essentials and Clinical Neurologic Applications. Radiology. 2021;299(1):3-26.
23. De A, Grenier J, Wilman AH. Simultaneous time-of-flight MR angiography and quantitative susceptibility mapping with key time-of-flight features. NMR Biomed. 2024;37(4):e5079.
24. Knobloch G, Nagle S, Colgan T, et al. Feasibility and optimization of ultra-short echo time MRI for improved imaging of IVC-filters at 3.0 T. Abdom Radiol (NY). 2021;46(1):362-372.
25. Schmidt VF, Dietrich O, Kazmierczak PM, Seidensticker M, Ricke J, Armbruster M. Optimized visualization of focal liver lesions and vascular structures in real-time T1-weighted gradient echo sequences for magnetic resonance-guided liver procedures. Diagn Interv Radiol. 2023;29(1):128-137.
26. Epstein FH, Mugler JP, Brookeman JR. Spoiling of transverse magnetization in gradient-echo (GRE) imaging during the approach to steady state. Magn Reson Med. 1996;35(2):237–245.
27. Jeon I, Cho ES, Kim JH, Kim DJ, Yu JS, Chung JJ. Feasibility of 10-Minute Delayed Hepatocyte Phase Imaging Using a 30° Flip Angle in Gd-EOB-DTPA-Enhanced Liver MRI for the Detection of Hepatocellular Carcinoma in Patients with Chronic Hepatitis or Cirrhosis. PLoS One. 2016;11(12):e0167701.
28. Schmidt VF, Dietrich O, Kazmierczak PM, Seidensticker M, Ricke J, Armbruster M. Optimized visualization of focal liver lesions and vascular structures in real-time T1-weighted gradient echo sequences for magnetic resonance-guided liver procedures. Diagn Interv Radiol. 2023;29(1):128-137.
29. Zibetti MVW, De Moura HL, Keerthivasan MB, Regatte RR. Optimizing variable flip angles in magnetization-prepared gradient-echo sequences for efficient 3D-T1ϱ mapping. Magn Reson Med. 2023;90(4):1465-1483.
30. Knobloch G, Colgan T, Wang X, Woo KM, Schubert T, Reeder SB. Combined gadoxetic acid and gadobenate dimeglumine enhanced liver MRI: a parameter optimization study. Abdom Radiol (NY). 2020;45(1):220-231.
31. Hellms S, Gutberlet M, Peperhove MJ, et al. Applicability of readout-segmented echoplanar diffusion weighted imaging for prostate MRI. Medicine (Baltimore). 2019;98(29):e16447.
32. Okada, Masahiro et al. “Optimal flip angle of Gd-EOB-DTPA-enhanced MRI in patients with hepatocellular carcinoma and liver metastasis.” Abdominal imaging vol. 39,4 (2014): 694-701.
33. Odin, Christophe. “Repetitive experiments of one or two-pulse sequences in NQR of spins I=3/2: Liouville space, steady-state, Ernst angle and optimum signal.” Solid state nuclear magnetic resonance vol. 85-86 (2017): 25-33.
34. Cai, Zhenyu et al. “Knee osteochondral junction imaging using a fast 3D T_1-weighted ultrashort echo time cones sequence at 3T.” Magnetic resonance imaging vol. 73 (2020): 76-83.
35. Xiao, Yu-Dong et al. “MRI contrast agents: Classification and application (Review).” International journal of molecular medicine vol. 38,5 (2016): 1319-1326.
36. Siedek, Florian et al. “Magnetic Resonance-Guided High-Intensity Focused Ultrasound (MR-HIFU): Technical Background and Overview of Current Clinical Applications (Part 1).” “Magnetresonanz-gesteuerter hochintensiver fokussierter Ultraschall (MR-HIFU): Technische Aspekte und Überblick über die etablierten Applikationen (Teil 1).” RoFo : Fortschritte auf dem Gebiete der Rontgenstrahlen und der Nuklearmedizin vol. 191,6 (2019): 522-530.